An Integrated System for the Study of Wind-Wave Source Terms in Finite-Depth Water

IAN R. YOUNG,* MICHAEL L. BANNER,+ MARK A. DONELAN,# ALEXANDER V. BABANIN,@ W. KENDALL MELVILLE,& FABRICE VERON,** AND CYRIL MCCORMICK#

*Swinburne University of Technology, Melbourne, Victoria, Australia
+School of Mathematics, University of New South Wales, Sydney, New South Wales, Australia
#Rosenstiel School of Marine and Atmospheric Science, University of Miami, Miami, Florida
@School of Civil and Environmental Engineering, University of Adelaide, South Australia, Australia
&Scripps Institution of Oceanography, University of California, San Diego, La Jolla, California
**College of Marine Studies, University of Delaware, Newark, Delaware

(Manuscript received 19 August 2002, in final form 29 January 2004)

ABSTRACT

A field experiment to study the spectral balance of the source terms for wind-generated waves in finite water depth was carried out in Lake George, Australia. The measurements were made from a shore-connected platform at varying water depths from 1.2 m down to 20 cm. Wind conditions and the geometry of the lake were such that fetch-limited conditions with fetches ranging from approximately 10 km down to 1 km prevailed. The resulting waves were intermediate-depth wind waves with inverse wave ages in the range $1 < U_{10}/C_p < 8$. The atmospheric input, bottom friction, and whitecap dissipation were measured directly and synchronously by an integrated measurement system, described in the paper. In addition, simultaneous data defining the directional wave spectrum, atmospheric boundary layer profile, and atmospheric turbulence were available. The contribution to the spectral evolution due to nonlinear interactions of various orders is investigated by a combination of bispectral analysis of the data and numerical modeling. The relatively small scale of the lake enabled experimental conditions such as the wind field and bathymetry to be well defined. The observations were conducted over a 3-yr period, from September 1997 to August 2000, with a designated intensive measurement period [the Australian Shallow Water Experiment (AUSWEX)] carried out in August–September 1999. High data return was achieved.

1. Introduction and aims of the project

The evolution of wind-generated waves in water of finite depth can be described by the wave action E/ω balance equation

$$\left[\frac{\partial}{\partial t} + (\mathbf{c}_g + \mathbf{U}) \cdot \frac{\partial}{\partial \mathbf{x}} - \nabla\Omega \cdot \frac{\partial}{\partial \mathbf{k}}\right] \frac{E}{\omega} = S_{\text{in}} + S_{\text{nl}} + S_{\text{ds}} + S_{\text{bf}}, \quad (1)$$

where the left-hand side represents the evolution of the wave action density as a result of the physical processes of atmospheric input from the wind, S_{in}; nonlinear interactions of various orders within the spectrum, S_{nl}; dissipation due to "whitecapping," S_{ds}; and decay due to bottom friction, S_{bf}. The directional spectrum is $E(f, k, \theta)$, the wave frequency is represented by $f = (\omega/2\pi)$, the wavenumber by k, and the direction of propagation by θ; $\mathbf{U}$ is the surface current and $\Omega(\mathbf{k}) = \omega(k) + \mathbf{k} \cdot \mathbf{U}$.

Under deep-water conditions, the evolution of the spectrum $E(f, \theta)$ for idealized fetch-limited conditions is reasonably well known (Donelan et al. 1985; Babanin and Soloviev 1998). Knowledge of the source terms on the right-hand side of Eq. (1) is, however, much more limited, particularly for finite-depth conditions (see, e.g., Young 1999). Spectral distribution of whitecapping dissipation has not previously been obtained, either experimentally or theoretically, and currently speculative approaches are used to represent this term in wave models. The natural phenomena determining this term are random, nonlinear, and sometimes related to extreme wave conditions and hence are difficult to evalu-

Corresponding author address: Alexander V. Babanin, School of Engineering and Science, Swinburne University of Technology, Melbourne, VIC 3122, Australia.
E-mail: ababanin@swin.edu.au

© 2005 American Meteorological Society

Unauthenticated | Downloaded 10/04/22 07:42 PM UTC

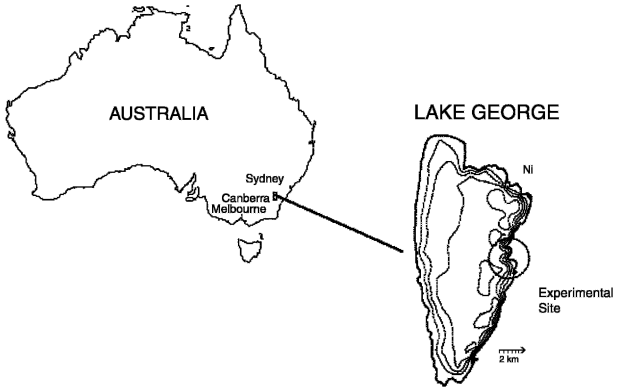

FIG. 1. Location of the Lake George site. Contour map of Lake George with the experimental site shown on the eastern shore of the lake. The contour interval is 0.5 m, and the maximum contour shown is 2 m. A detailed survey of the area near the experimental site indicates that the bathymetry is much simpler than shown on this map. The compressed contours in the region are an artifact of the contouring routine used.

ate in the field. The bottom-dissipation and wind-input terms have been the subjects of intensive research during the last three decades, although detailed field observations are rare. However, while there is a qualitative understanding of their behavior, no established quantitative description is available.

In 1990–94 a major finite-depth field experiment was conducted in Lake George, near Canberra, Australia. Lake George is a large shallow lake (20 km $\times$ 10 km, with water depth varying seasonally from 2 m down to 0.2 m), ideally suited to investigating fetch-limited spectral evolution in finite-depth water [Fig. 1, reproduced from Fig. 1 in Babanin et al. (2001)]. The wave spectrum and meteorological conditions were measured at a series of eight locations at fetches ranging from 1.5 to 16 km. As a result of these measurements, a detailed understanding of the spectral evolution in finite-depth water has resulted. The results of this study can be summarized as follows.

- Nondimensional growth curves for energy and peak frequency were developed as a function of fetch.
- The spectral shape in finite-depth water was confirmed to be approximately that described by Bouws et al. (1985) (i.e., based on TMA dataset)
- The evolution of all the spectral parameters describing this finite-depth spectral form were parameterized.
- The directional spectrum was shown to be broader in finite-depth conditions than in deep water.
- The directional spreading was parameterized in terms of f/f_p, where f_p is the frequency of the spectral peak.

The full experimental description and results have been presented by Young and Verhagen (1996a,b), Young et al. (1996), and Young et al. (1997). The Lake George results were far more comprehensive than previous finite-depth studies (i.e., Bretschneider 1958; Bouws et al. 1985), although they were consistent with these studies. This occurred despite the fact that the various studies were conducted in a variety of geographical locations (i.e., lakes, coastal sites, and shallow seas), presumably with a variety of different bed materials. Extrapolation of the deep-water source terms of Eq. (1) to finite-depth situations indicated that all source terms should be of comparable magnitude. Our knowledge of the bottom-friction source term (S_{bf}), the best known of the finite-depth terms, suggested that it can vary by an order of magnitude with relatively small changes in the bed material. Hence, one would conclude that the resulting spectral evolution should also vary significantly with geographic location. As this was inconsistent with the field observations, a reassessment of the relative magnitude of the source terms in finite-depth situations was also required.

The aim of the Lake George project, described in this paper, was to measure as many of the source terms in Eq. (1) as possible under various fetch-limited conditions. All the measurements were simultaneous and synchronized. As the spectral evolution of the directional spectrum is already established from the extensive previous measurements conducted at Lake George, such measurements provide a unique opportunity to close the energy balance. Effectively, both sides of the governing equation will have been measured in the finite-depth conditions of Lake George.

An integrated set of measurements in the atmospheric and subsurface boundary layers, as well as on the surface itself, was carried out at the Lake George field experimental site from September 1997 to August 2000, whenever meteorological forecasts were appropriate. In August–September 1999, the end of the Southern Hemisphere winter and a time of regular strong cross-lake winds, an intensive observation period was conducted. For this period, the measurement systems were supplemented by finescale measurements of wave-induced air pressure, subsurface turbulence, and bottom boundary layer velocity profiles. This latter experiment was titled the Australian Shallow Water Experiment (AUSWEX).

AUSWEX was followed by two sets of laboratory experiments at the School of Civil Engineering at the Australian Defence Force Academy (ADFA) to improve estimates of the wave energy dissipation due to interaction with the lake bed.

Unauthenticated | Downloaded 10/04/22 07:42 PM UTC

2. The experiment

A contour map of Lake George is shown in Fig. 1. The bathymetry of the lake is very simple, with the bed sloping gently toward the eastern shore. As a result of the extensive meteorological data obtained during the 1990–94 experiment it was clear that prevailing winds were from the west. Therefore, fetch-limited finite-depth waves commonly occur along the eastern shoreline, where the new experimental site was constructed. In addition, as the lake bed is extremely flat, refraction effects would be insignificant, thus simplifying the governing equation. The lake bottom in the region of the observation site was remarkably flat, with a slope of 2×10^{-4}, and no small-scale undulations. Under typical meteorological conditions the range of values of inverse wave age, U_{10}/C_p, and nondimensional depth, $k_p d$, that could be expected at the site were $1 < U_{10}/C_p < 8$ and $0.5 < k_p d < 3$, respectively. Hence, the experimental conditions were representative of intermediate-depth wind seas.

a. Facility design

Experience gained during the 5-yr (1990–94) measurement program at Lake George had shown the enormous difficulty of operating manned experiments in wind conditions in excess of 8 m s^{-1}. The steep wind seas that develop in the shallow waters make operation of small boats difficult and at times hazardous. Consequently, experimental design for the new site was based around the construction of a shore-connected platform in finite-depth water but beyond the surf zone. Careful surveys of the eastern shoreline led to the choice of the site shown in Fig. 1. This location had vehicular access and a simple offshore bathymetry. At the beginning of the project in 1997, the water was approximately 1.5 m in depth within 50 m of the shoreline. As Lake George was going through its regular hydrological cycle, the depth dropped down to 20 cm by the end of the experiment in late 2000. Therefore, the slow variation of the water depth, combined with the associated changes in fetch, provided a range of observational conditions.

An elevated walkway was built from the shore to a small research platform approximately 50 m offshore (Fig. 2). The walkway was fabricated from construction scaffolding and terminated in a platform approximately 4 m $\times$ 3 m in size. Under the very common westerly winds, waves at the platform were fetch limited and finite depth, and closely approximated idealized fetch-limited wave growth. They were not, however, within the surf zone. As the platform was shore-connected, access was possible even in the most severe meteorological conditions.

FIG. 2. View of the experimental site with elevated walkway, observational platform with computer shed on it, and suspended measurement bridge. The photo was taken before 1998, when the second anemometer mast was erected away from the bridge.

The observational platform was provided with a shelter to accommodate electronics and equipment, as well as researchers, during observational periods. A measurement bridge was constructed northward from the platform; it served as a frame for the majority of the wave measurements but did not disturb the surface and the water underneath [Fig. 3, reproduced from Fig. 2 in Babanin et al. (2001)]. Two anemometer masts are also seen in this picture; they will be described in detail in section 3b and were dedicated to the atmospheric measurements.

Two shelters constructed onshore provided basic storage and accommodation for researchers during their stay at the site. Shore-based generators supplied

FIG. 3. Offshore view of the experimental site. The platform, computer shed, measurement bridge, and anemometer masts are seen. The device in the foreground is a mobile single-probe wave array.

Unauthenticated | Downloaded 10/04/22 07:42 PM UTC

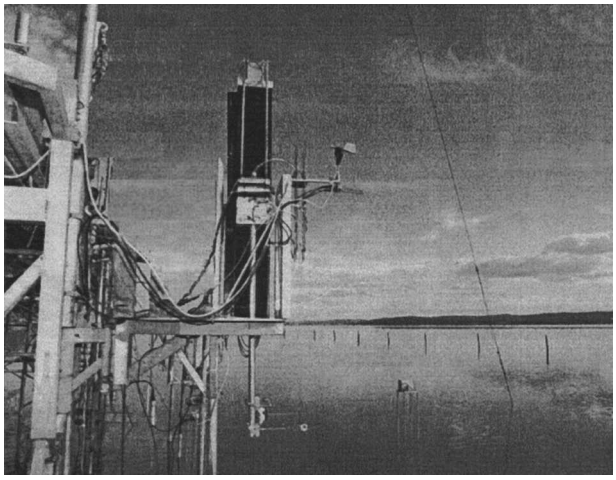

FIG. 4. The wave follower shown positioned at the measurement bridge during AUSWEX.

240 V of power to the facility and platform computers and instrumentation. The location had vehicular access, and computer facilities allowed for preliminary data analysis to be performed on site, although the main data processing was conducted at a later time. The site was located approximately one hour's drive from ADFA, and the measurements were performed whenever meteorological conditions were appropriate.

b. AUSWEX

The Australian Shallow Water Experiment was conducted in August and September 1999 when the mean water depth at the experimental site was approximately 40 cm. In addition to measurements of the directional wave spectrum, meteorological conditions, frequency and strength of wave breaking, and turbulence within the water column, which were performed in the extended 1997–2000 period, detailed measurements in the atmospheric boundary layer very close to the water surface were carried out by means of a wave follower, designed at the University of Miami, Florida (Donelan et al. 2005). Measurements of the spatial distributions of water turbulence were also performed, with the aid of a coherent acoustic Doppler ("Dopbeam") device provided by the Scripps Institution of Oceanography, California (Veron and Melville 1999). Profiling of the bottom boundary layer was conducted with a higher-resolution acoustic Doppler velocimeter (ADV) and a high-precision vertical traversing system designed by the School of Civil Engineering, ADFA (Mirfenderesk and Young 2004).

The wave follower was the primary system to enable direct measurements of the wind input. In Fig. 4 [reproduced from Fig. 3a in Donelan et al. (2005)], it is shown positioned at the measurement bridge during AUSWEX. As can be seen, the follower was installed on a rotating platform that allowed for changes in the orientation of the follower's probe so as to align the instruments optimally with the wind and wave directions. Details of the wave-follower measurements can be found in Donelan et al. (2005) and are summarized in the atmospheric measurements section (3b).

The Dopbeam is a pulse-to-pulse coherent acoustic Doppler profiler for the measurement of spatial distributions of turbulence (Veron and Melville 1999). The device was deployed under the measurement bridge, near the other subsurface turbulence instrumentation, to provide a reference value of dissipation rates for vertical profiles of the integral dissipation, obtained by the vertical array of ADVs (see section 3c).

3. Measurements and instrumentation

An integrated set of measurements in all four relevant environments (the atmospheric boundary layer, the water surface, the water column, and the bottom boundary layer) was carried out at the Lake George field experimental site to obtain the necessary source functions of Eq. (1), as described in the following subsections. All the measurements were synchronized, and the water surface of the main measurement area was synchronously videotaped (section 3f).

a. Surface wave field

All the source terms are functions of the surface wave conditions, a full representation of which requires high-resolution measurements of the directional spectrum. To obtain measurements of the directional spectrum, a spatial array of capacitance gauges in the form of a centered pentagon with 15-cm diameter was used. The array was deployed at the middle of the measurement bridge, sufficiently far from any disturbances of the water surface caused by the construction scaffolding.

Two further capacitance elements were located in close proximity to the central element of the array to provide measurements of the mean-squared surface slope (thus the three central probes formed a right triangle with 4-cm side). Although it has yet to be confirmed, both atmospheric input and dissipation may be functions of this quantity. Also, the inner array of three probes served as an independent tool to measure directional spectra of short waves (Babanin et al. 1999). Therefore, the array effectively consisted of eight wave probes. In Fig. 5a, the geometry of the array is seen, and in Fig. 5b, the location of the array under the suspended bridge is shown.

Unauthenticated | Downloaded 10/04/22 07:42 PM UTC

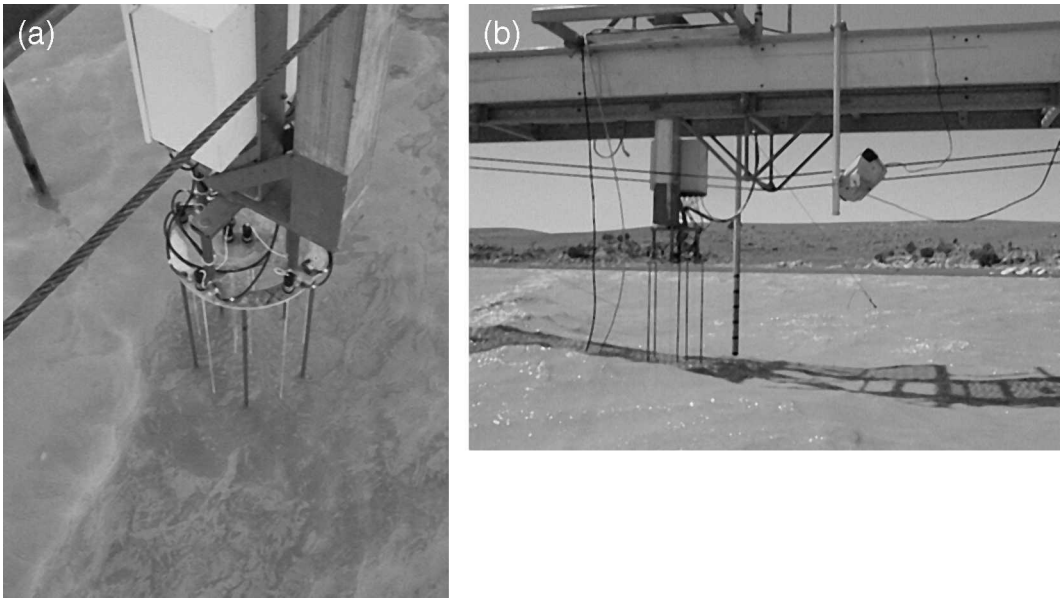

FIG. 5. (a) Wave array positioned under the measurement bridge. Geometry of the array, consisting of the external centered pentagon and internal triangle wave-slope array, is seen. Control units are placed in the rectangular box on the top of the array. (b) Location of the wave array viewed by the synchronized water-protected video camera. Shaft behind the array holds submerged vertical array of ADVs. Cables connecting the collocated hydrophone at the bottom of the array and video camera with the main logging system are also seen.

The array was composed of capacitance wave height gauges manufactured by Richard Brancker Research, Ltd., Canada. The sensing probes were Teflon-coated wires, 1 m long and 1 mm thick. Manufacturer specifications guaranteed 0.2% linearity and 0.4% accuracy, as well as a 2-ms time response. For the Lake George measurements a Brancker model WG-30 system was used, which was designed to operate in a master/slave time-sequenced format so that two or more probes could be positioned together (less than 100 cm apart) and still avoid interference. Since the probes were positioned much closer than 100 cm, thorough laboratory tests were performed at ADFA with the prepared array prior to its field deployment to verify that interference effects were negligible. In addition, accurate calibrations were done at the laboratory, and facilities for quick calibration in the field were set up at the measurement platform. Calibrations were performed frequently. Calibration characteristics of the gauges proved remarkably stable during the 3-yr-long experiment.

Considerable experience had been gained by the participants in the analysis of data from such arrays using the maximum likelihood method (MLM) (Young 1994; Young et al. 1996; Babanin and Soloviev 1998; Babanin et al. 1999). Furthermore, the wavelet-based wavelet directional method (WDM) developed by Donelan et al. (1996), which also enables the measurement of the temporal evolution of the directional wavenumber spectra, has been successfully applied to the Lake George data. The wave array data and the directional analysis methods used allowed recovery of directional spectra of wind waves at all scales of interest: from 10–15-m-long waves (the longest detected during the Lake George experiment) down to waves of some 10 cm in wavelength. An example of a directional spectrum measured by the three-wire internal array is shown in Fig. 6 [reproduced from Babanin et al. (1999)], where fine features, such as bimodality of the spectrum at higher frequencies, can be seen.

The array provided reliable but single-point measurements of the wave spectra. Therefore, three mobile wave arrays were deployed to investigate spatial effects of small-scale spectral and group variability. These effects include advection, evolution of wave groups and waves within the groups, and measurement of breaking waves at different phases of the breaking process. The arrays were constructed as sensing wires between thin metal frames. The shallowness of the lake allowed for simple mounting of the mobile arrays on the lake bottom at different distances from the main array. The mobile arrays were connected by cable to the main logging system. Their distance from the main array was varied from a few meters to a few tens of meters, depending on the task being considered. Two single arrays, with capacitance wave gauges WG-30, and one

Unauthenticated | Downloaded 10/04/22 07:42 PM UTC

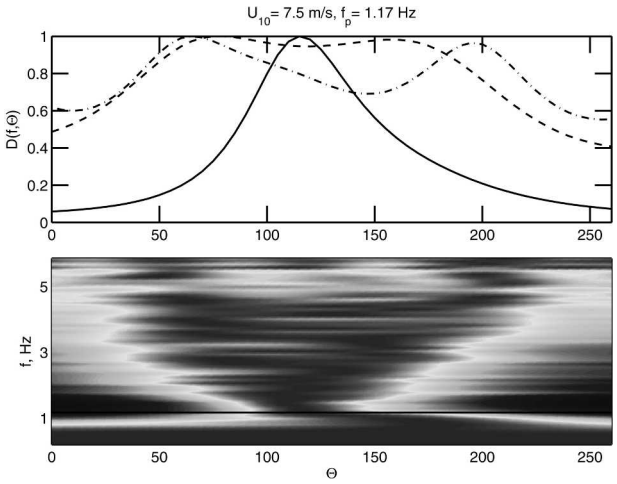

FIG. 6. Example of a directional distribution showing bimodal spreading. (top) Two-dimensional sections at f_p (solid line), $2f_p$ (dashed line), and $3f_p$ (dash–dotted line) frequencies. (bottom) Color-shaded image of the directional spreading. Frequency spectral peak is indicated by straight line across the directional span.

array of three resistance probes, consisting of a loop of wire with vertical arms separated by 3 cm, were used for these purposes. One of the single arrays is seen in the foreground of Fig. 3 and in background of Fig. 4. The mobile arrays were also frequently calibrated in the field: calibration of the resistance probe array proved less reliable than that of the capacitance probe and varied with time.

The wave-follower system, deployed during AUSWEX, had separate and independent means of wave spectra measurement: resistance probes used to drive the follower's position, an array of three capacitance probes, and an array of three bottom pressure gauges. They were mainly used for the AUSWEX wind-input study and are described in detail in Donelan et al. (2005).

b. Determination of atmospheric input

The atmospheric input from the wind is the only source function of Eq. (1) that can be measured directly. This is achieved by measuring the wave-induced pressure in the air, immediately above the water surface. It is the component of pressure in quadrature with the water surface that is primarily responsible for the transfer of energy from the wind to the waves (Snyder et al. 1981; Donelan 1999). Hence, it is necessary to measure simultaneously both the water surface elevation and the air pressure. Ideally, this should be achieved with a pressure probe moving in a wave-following coordinate system. This necessitates the use of a wave follower that can hold a pressure probe at a fixed distance above the "randomly" moving water surface. This should be done with minimal amplitude and phase errors (Young and Sobey 1985; Donelan et al. 1999).

A high-precision electromechanical servo-feedback system, developed at the University of Miami, Florida, was utilized for the wave follower during the AUSWEX part of the Lake George experiment. The precision of the feedback wave-following mechanism did not impose any restrictions on the measurement accuracy in the range of wave heights and frequencies relevant to the problem. To the accuracy with which it could be measured, the transfer function had a gain of 1.0 and a phase lag of 0° in this range.

The principal sensing hardware included Elliott pressure probes (Elliott 1972), hot-film anemometers, and Pitot tubes. An Elliott pressure disk that has essentially zero dynamic velocity response was used for the purpose of measuring pressure pulsations in the moving coordinate system. The hot films and Pitot tubes provided independent estimates of wave-induced stresses by means of measuring pulsations of vertical and horizontal velocity close to the water surface: they were mounted both on the moving arm and stationary body of the follower. In Fig. 4, an Elliott probe disk can be seen at the very bottom of the following arm, with holders for the hot films and a Pitot tube above the Elliott probe. A pair of hot-film and Pitot tube holders are seen at the top of the follower, near the wind vane. The water surface was sensed by a pair of resistance wires located on either side of the Elliott pressure-sensing probe. Calibrations of the pressure transducers and moving Elliott probes were conducted, as well as regular calibrations of the resistance wave gauge. Spectral distributions of the momentum input were verified by means of independent measurements of the integrated air–water fluxes. Postexperiment laboratory tests of the wave-following instrument were conducted, which showed that the response of the air column in the connecting tubes provides a frequency-dependent phase shift, which must be accounted for to recover the low-level induced pressure pulsations. More details of this part of the atmospheric input study, as well as an example of the measured wind-input spectral function, can be found in the companion paper by Donelan et al. (2005).

An ongoing debate exists among wave researchers as to whether S_{in} should be parameterized in terms of the wind speed at a fixed reference height, U_{10}, or the friction velocity, u_*, or the wind speed at a height dependent on the wavelength, $U_{\lambda/2}$, where λ is the wavelength (Donelan 1990). Previous experiments, which had measured S_{in}, had not measured all these boundary layer

Unauthenticated | Downloaded 10/04/22 07:42 PM UTC

parameters to determine the most appropriate representation. The Lake George experiment was designed to allow the measurement of all relevant boundary layer properties.

An anemometer mast, accommodating three wind probes (two cup anemometers and one directional vane) at 10- and 5.65-m elevations over the water surface, was erected 10 m from the platform at the end of the measurement bridge. Another anemometer mast, accommodating four cup anemometers and one directional vane at four heights closer to the surface, was set 6 m off the bridge to ensure undisturbed airflow for these lower anemometers. In total, the wind profile was measured at six heights, logarithmically spaced from 10 m down to 22 cm above the mean water level. The wind direction was measured at 10- and 0.89-m heights, and gust values were recorded at four levels. The two anemometer masts can be seen in Fig. 3, only the top speed and directional anemometers at 10-m height being out of sight. Slow changes in the water depth in Lake George caused small variations in the position of the sensors relative to the surface, and corresponding adjustments in the U_{10} speed estimates were made on the basis of the wind profiles obtained with the anemometer mast.

The wind probes were Aanderaa Instruments Wind Speed Sensor 2740 and Wind Direction Sensor 3590. The wind speed sensor consists of a three-cup rotor on top of an aluminum housing, with a threshold speed less than 0.4 m s^{-1}, and is capable of measuring wind speeds up to 76 m s^{-1}. Its accuracy is $\pm 2\%$ or ± 0.2 m s^{-1}, whichever is greater. The sensors provide two output quantities within each sampling interval: a 1-min-average wind speed and wind gust, the latter being defined as the highest speed occurring over a 2-s period at any time during the sampling interval. The sampling interval chosen was 1 min. The rotor bearings consist of two stainless steel ball bearings, and during the 3-yr experiment, the bearings of only one of the probes failed and had to be replaced. At the end of the experiment, the sensors were calibrated in the wind tunnel of the School of Aerospace and Mechanical Engineering, ADFA, with the calibration curves for all the probes being found to be very close to the original manufacturer's calibrations.

The wind direction sensor consisted of a light wind vane pivot on top of a housing. Inside the housing a compass is magnetically coupled to the vane. The threshold speed for the meter is 0.3 m s^{-1}, and the accuracy is $\pm 5°$. An Aanderaa Sensing Scanning Unit 3010 was used to negotiate between the probes and the main logging computer. The unit was capable of scanning 12 channels, and therefore six profile wind speeds, four profile wind gusts, and two profile wind directions were logged every minute.

An example of 10 consecutive 1-min-averaged profiles of a record with 8.4 m s^{-1} mean U_{10} wind speed is shown in Fig. 7 to demonstrate the capability of the anemometer mast. Clearly, the mast is not only capable of measuring mean values of the above mentioned U_{10}, u_*, and $U_{\lambda/2}$, but also their variations at time scales greater than 1 min.

Redundancy was built into the boundary layer measurements to allow for multiple cross-checks of the results and characteristics. The friction velocity u_*, obtained from the wind profiles, can also be measured using a sonic anemometer: $u_*^2 = -u'w'$, where u' and w' are oscillations of the horizontal and vertical velocity, respectively. A Gill Instruments Solent Research Ultrasonic Anemometer was deployed for this purpose. The device sampled the three-dimensional air velocity fluctuations at 21-Hz frequency and has instantaneous accuracy of $\pm 3\%$ for wind speeds less than 30 m s^{-1}. This instrument works for speeds up to 60 m s^{-1} and is extremely rugged and capable of operation in the most severe meteorological conditions. During the 3-yr observational period, the anemometer was once shipped to the manufacturer to check its calibration characteristics, which were found to be within specifications. In Fig. 3, the sonic anemometer is seen positioned vertically at the anemometer mast above the measurement bridge. During AUSWEX, it was moved to the top of the distant anemometer mast to avoid possible air disturbances by the bridge.

Independent measurements of stresses and fluxes in the air were also provided by the wave-follower system's hot films and Pitot tubes, as mentioned above and described in Donelan et al. (2005).

c. *Determination of breaking statistics and dissipation in the water column*

The dissipation term is intrinsically difficult to measure directly. As most of the wave energy dissipation is associated with "whitecapping," or wave breaking, knowledge and understanding of the breaking process is only fragmentary. The strongly intermittent and nonlinear character of the breaking phenomenon creates profound complications for theoretical approaches to these problems. At the same time, field observations of breaking waves encounter logistical difficulties since the most important situations of extreme seas are usually the least accessible to systematic measurement. Even when reliable wave data are obtained, the absence of established breaking criteria in such measurements makes it difficult to detect particular breaking events within these data records. Prior to the Lake

Unauthenticated | Downloaded 10/04/22 07:42 PM UTC

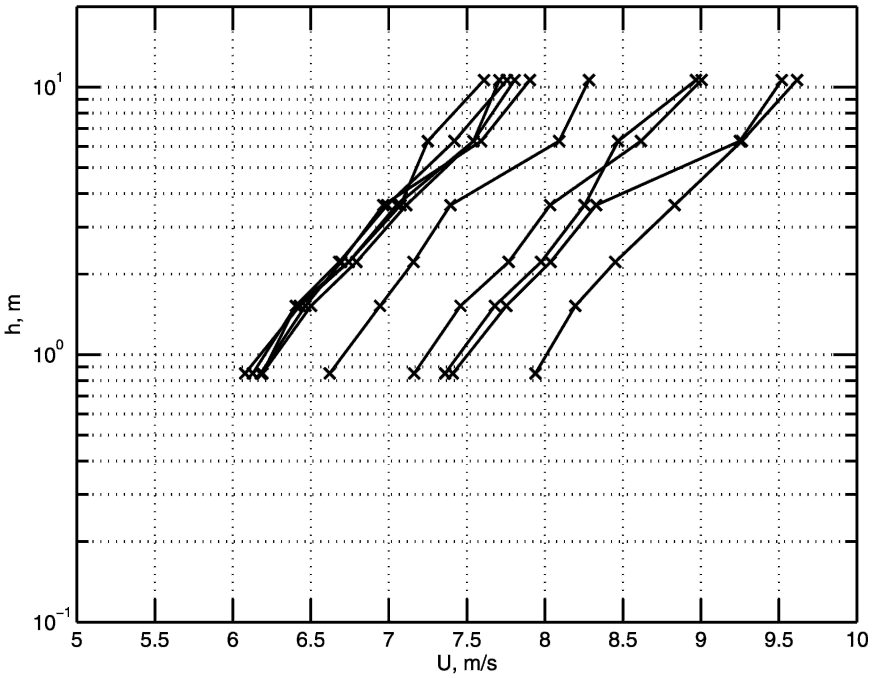

FIG. 7. Ten consequent 1-min-average wind profiles measured by the anemometer mast. Crosses indicate positions of the wind speed sensors.

George study, there were no widely accepted breaking criteria and no reliable breaking detection method. No systematic breaking statistics in relation to wave characteristics and environmental forcing had been obtained, and consequently no nonspeculative dissipation spectral term S_{ds} had been established.

Even a reliable determination of the total dissipation rate (much less its distribution with frequency) had, until recently, been elusive. In complementary articles, Terray et al. (1996) and Drennan et al. (1996) have reported measurements of the variation of energy dissipation rate with depth below the water surface in the presence of actively breaking wind waves. From such measurements of the dissipation rate profile, the total dissipation rate was estimated. An alternative method was suggested by Melville et al. (1988; see also Loewen and Melville 1991), whose laboratory investigation demonstrated a close correlation between the dissipation of wave energy associated with breaking, and the acoustic output of individual breaking waves.

The Lake George experiment targeted both experimental problems: measurements of the spectral distribution of wave energy dissipation due to wave breaking and, as a consistency check, independent measurements of the total energy dissipation in the water column. As with the wind-input measurements, techniques adopted were intended to incorporate redundancy into breaking out wave dissipation measurements by deploying complementary instrumentation and allowing for multiple cross-checking of measured properties. This composite monitoring of whitecapping events provides unique data on the largely unexplored process of shallow-water wave breaking.

1) WAVE-BREAKING MEASUREMENTS

To measure whitecapping dissipation, four different but integrated instrument systems were employed. Since individual waves naturally change their heights while propagating within irregular wind-wave groups, direct in situ estimates of energy lost by breaking were obtained in terms of the integrated group energy, measured with the array of capacitance wave probes. Since the integrated group energy should be measured before and after a breaking occurred within the group (e.g., Rapp and Melville 1990), three additional mobile wave arrays were positioned to measure spatial decay of breaking wave groups, as described in section 3a. Orientation of the set of wave arrays was chosen on an individual day so as to align with the main wave direction. The distances between the arrays were varied from a few meters to a few tens of meters.

Identification of wave groups containing breaking waves was a crucial component of these measurements, and video records, synchronized with the wave records,

Unauthenticated | Downloaded 10/04/22 07:42 PM UTC

FIG. 8. Subsurface hydrophone housing. The sensing head is seen on the right. On the top of the housing, there are waterproof connectors for the cables.

were used for this purpose (see section 3f). The video camera is shown in Fig. 5b recording the location of the main stationary array. To observe the wave group evolution, the video camera was positioned at a higher elevation, such that all the mobile and stationary arrays were in sight.

In addition, breaking events were recorded visually by an observer, who marked them (or other events of interest) electronically. The observer would watch a designated location from the platform and trigger an electronic signal to register the passage of a whitecap past a chosen wave probe. The electronic signal was recorded on a separate channel of the main logging system, synchronously with all other records.

A primary sensing device for the breaking wave studies was an underwater hydrophone, the output of which was related to both the strength and dimension of breakers. The acoustic output of the subsurface hydrophone was recorded and, in most cases, video recording of the surface spot around the array was also performed to identify breaking events and to supply information on the spatial dimensions of whitecapping.

The hydrophone sensor was provided by the Australian Defence Science and Technology Organization (DSTO), and the preamplifier was designed and constructed by the School of Civil Engineering at ADFA. The hydrophone/preamplifier system was calibrated at DSTO, and its characteristics were found linear both in amplitude and frequency up to at least 20 kHz, which covered the entire range of interest (during subsequent data analysis the acoustic signal was sampled at an 8-kHz rate and digitized). The hydrophone's electronics and batteries were housed in a waterproof container (Fig. 8), with the hydophone's sensitive head visible outside the container. The hydrophone was located on the bottom beneath the array (see Fig. 5b, where cables, connecting the hydrophone to the main logging system, are visible).

The hydrophone output was recorded on an audio channel of the video system. The hydrophone had two signal gains, 20 and 40 dB. Normally, for developed wind waves the 20-dB gain was sufficient to detect breaking waves. The video recorder sent a time code to the data acquisition system and to the second audio channel of the video tape (see section 3f), so that precise correlation between whitecap events and the related data could be achieved. The synchronized time series of the hydrophone acoustic signal and the visual video record contain potentially valuable additional information about visually observed dominant wave breakers, particularly in relation to breaker strength.

Figure 9 is a spectrogram of 1 min of a hydrophone record. The spectrogram is a time series of consecutive spectral densities computed over 256 readings of the acoustic signal with a 128-point overlap. The segments were windowed with a Hanning window. Values of the spectral density are shown using a logarithmic scale, with darker patches corresponding to higher values (i.e., louder recorded sound levels). The dark crests across almost the entire 4-kHz frequency span in the spectrogram are associated with acoustic noise from dominant breaking waves. This was confirmed through repeated viewing of the synchronized video records. For example, the first and last breakers (near $t = 1$ s and $t = 55$ s) detected in the spectrogram in Fig. 9 are shown in the captured video images seen in Figs. 10a and 10b, respectively. It is clear that these are cases when the crest of a breaking wave is passing through the wave array and over the bottom-mounted hydrophone. Figures 9 and 10 are reproduced from Babanin et al. (2001), in which the breaking detection procedure is discussed in greater detail.

During AUSWEX, an HTI-96-MIN hydrophone manufactured by High Tech, Inc., Massachusetts (frequency response from 2 Hz to 30 kHz), was incorporated into the wave-following system for similar purposes. It was located on the bottom directly beneath the surface sensing spot, where the Elliott probe of the wave follower was measuring pressure in the air. The hydrophone was placed into a metal tube open upward so that its sensitive diaphragm was exposed to downward-propagating sound only. Hence it was sensitive only to breaking events occurring directly above—at the point where the wind input was being measured. Three pressure probes, positioned at the bottom in the vicinity of the wave-follower measurements, were also used for breaking detection purposes, as described by Donelan et al. (2005).

Unauthenticated | Downloaded 10/04/22 07:42 PM UTC

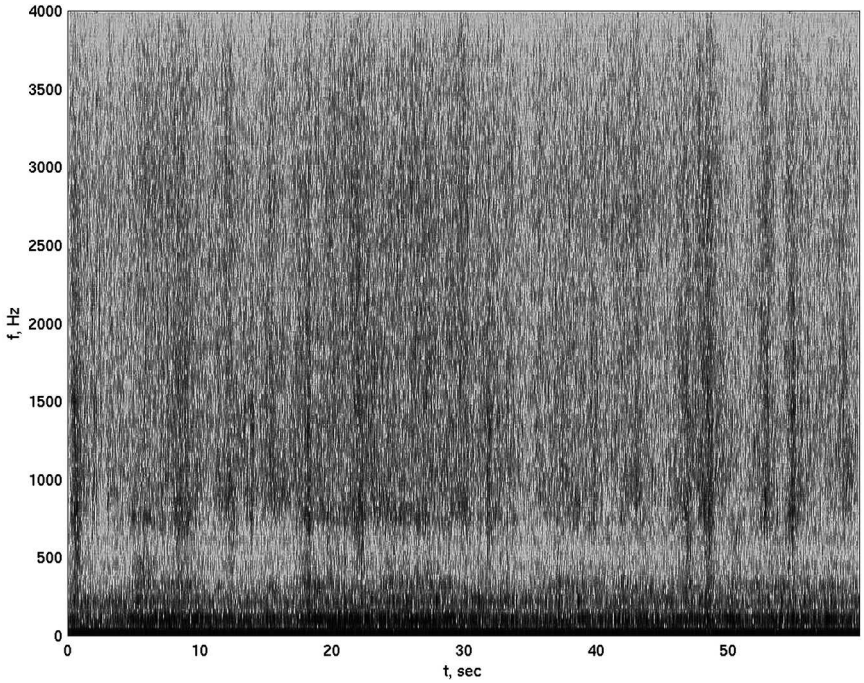

FIG. 9. Spectrogram of acoustic noise of a 1-min record. The dark crests across the frequency span are associated with acoustic noise from breaking waves.

2) TOTAL DISSIPATION MEASUREMENTS

Measurements of the profile of dissipation rate with depth were performed to obtain the total energy dissipation in the water column. For this purpose, Sontek ADVs were used to determine the turbulent velocities up to 12.5 Hz (sampling rate, 25 Hz), together with the analysis techniques described in Drennan et al. (1996).

The analysis techniques allow the determination of the dissipation rate per unit of volume at a particular depth, where the measurement volume of an ADV is located. To estimate the total dissipation, which should match the integral of S_{ds}, vertical profiles of the rate must be obtained, extrapolated to the surface, and integrated over the depth to give the total dissipation rate. Up to three ADV probes were mounted on a vertical traversing system so that data could be obtained for a range of depths. The vertical shaft, to which the ADVs were mounted, is shown in Fig. 5b behind the main array. The ADVs were always positioned such that they pointed into the waves so that the measurement volumes were located in the water body ahead of the probe, undisturbed by the presence of the ADV.

The Sontek ADV is a single-point, three-dimensional Doppler current meter. It performs velocity measurements in a sampling volume 5 or 10 cm away from emitting sound fingers. The default sampling volume is 9 mm in diameter but can be reduced to 1 mm if necessary. Due to configuration of the sound-emitting fingers, one of the velocity directions—along the main axis of the ADV—has a higher signal-to-noise ratio (at least by an order of magnitude in spectral terms). Of the three ADV probes deployed at Lake George, one was a 10-cm probe and the two others were 5-cm probes. The probes were oriented such that the axis with the highest signal-to-noise ratio was aligned with the wave propagation direction.

Examples of the ADV measurements of the dissipation rates are shown in Fig. 11. In Fig. 11a, a set of six velocity spectra, based on consecutive 20-min-long ADV records, taken on depths from 10 to 60 cm from the surface, is shown. The Kolmogorov turbulence tail, seen as proportional to $f^{-5/3}$ above $f \approx 2$ Hz, has a level depending on the energy dissipation rate ε. The level should rapidly decrease away from the surface (Craig and Banner 1994; Terray et al. 1996; Drennan et al. 1996), as it is the case in the figure. Figure 11b shows a number of ADV measurements plotted in "law-of-the-wall" coordinates (Soloviev et al. 1988). Here, κ is von Kármán's constant, u_{*w} is friction velocity in the water, and z is measurement depth. For a turbulent flow, the dimensionless dissipation rates should lie on the law-of-the-wall line. Clearly, apart from some outliers, there is significant enhancement of the dissipation above this level. Agrawal et al. (1992), Melville (1994),

Unauthenticated | Downloaded 10/04/22 07:42 PM UTC

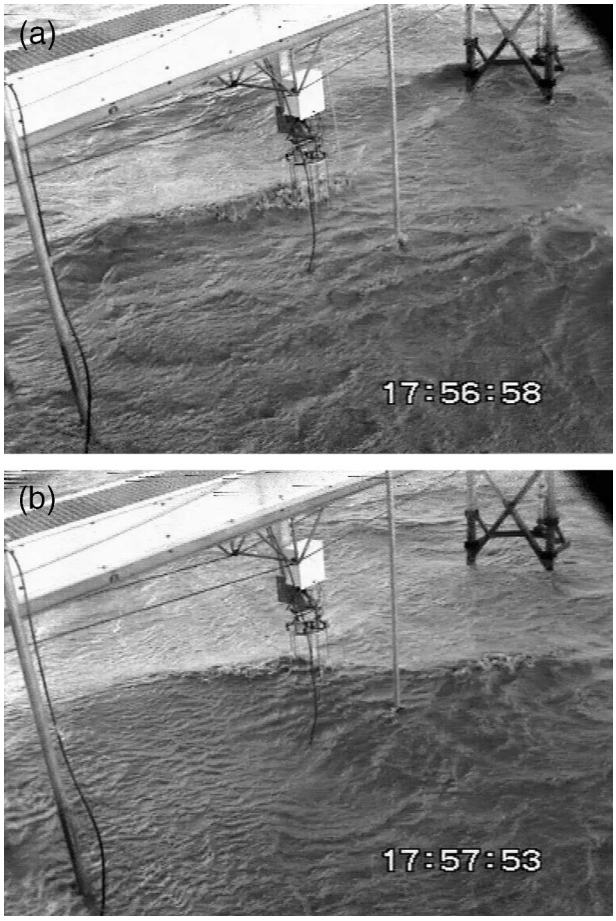

FIG. 10. (a) Video image of the breaker occurring near $t = 1$ s of the record in Fig. 9. (b) Video image of the breaker occurring near $t = 55$ s of the record in Fig. 9.

Terray et al. (1996), and Drennan et al. (1996) attribute this to enhancement by wave breaking.

3) MEASUREMENTS OF TURBULENCE PROFILE

The technique used by Drennan et al. (1996) requires knowledge of the advective velocity of the turbulence to convert measured single-point frequency spectra of turbulence into wavenumber spectra. The normal assumption is "frozen turbulence," with the advection velocity being the rms of the orbital velocity of the surface waves (Lumley and Terray 1983). The requirement for such an assumption can be avoided if the wavenumber spectrum can be measured directly. An acoustic Doppler profiler (Dopbeam) was used during AUSWEX to directly obtain turbulence wavenumber spectra and therefore provide a reference spectrum for the ADV measurements [section 3c(2)].

The Dopbeam is a 1.72-MHz, programmable, monostatic, single-beam sonar system performing pulse-to-pulse coherent Doppler measurements of the along-beam fluid velocity (Veron and Melville 1999). Typically, it operates in the range 0.5–5 m with a direct unambiguous velocity measurement between 0.3 and 0.03 m s^{-1}. For these experiments it was programmed to ping at a 625-Hz repetition rate, which was averaged down, yielding a final profiling rate of 25 Hz. Each profile was 1.2 m long and contains the one-dimensional, along-beam velocity component. Therefore, both instantaneous wavenumber spectra along the profile and frequency spectra at different distances from the emitter are available. The wavenumber spectra of turbulence are measured up to 300 rad m^{-1} or some 7 Hz in frequency, if converted.

The main advantage of the Dopbeam over conventional single-point velocity measurements is its spatial extent measurements so that wavenumber spectra could be calculated directly without invoking Taylor's hypothesis. Identifying the Kolmogorov inertial subrange and measuring the spectral level permits direct estimates of the turbulent kinetic energy dissipation ε. In addition, dissipation rates were estimated using the variance of the shear along the velocity profiles collected by the Dopbeam. These estimates were found to compare favorably (Veron and Melville 1999).

During AUSWEX the Dopbeam was positioned horizontally on a vertical traversing shaft. In most cases, it was oriented cross-wave to limit the effects of wave orbital motion on the measured instantaneous turbulence profiles. The Dopbeam shaft was located next to the main wave array but "looking" away from the array to avoid obstructions of the sonar beam. Dopbeam measurements at different depths, taken in stationary conditions, complemented the ADV measurements of vertical profiles of the dissipation rate ε. The Dopbeam wavenumber spectra, measured at various water depths, served as a reference for conversion of the ADV-measured frequency spectra recorded at the same depths to wavenumber spectra.

d. Determination of bottom friction

The existence of bottom interaction mechanisms in finite-depth conditions, such as friction, percolation, and scattering, has been recognized for some time (Weber 1991). To date, there have been few conclusive field measurements of these processes or laboratory measurements directly obtaining information on bottom friction through the measurement of the near-bottom oscillatory boundary layer. This type of measurement is difficult to make in the field and relies on the assumption of a friction law (usually quadratic) to obtain an estimate of the bottom friction decay.

It was proposed to overcome these problems by the

Unauthenticated | Downloaded 10/04/22 07:42 PM UTC

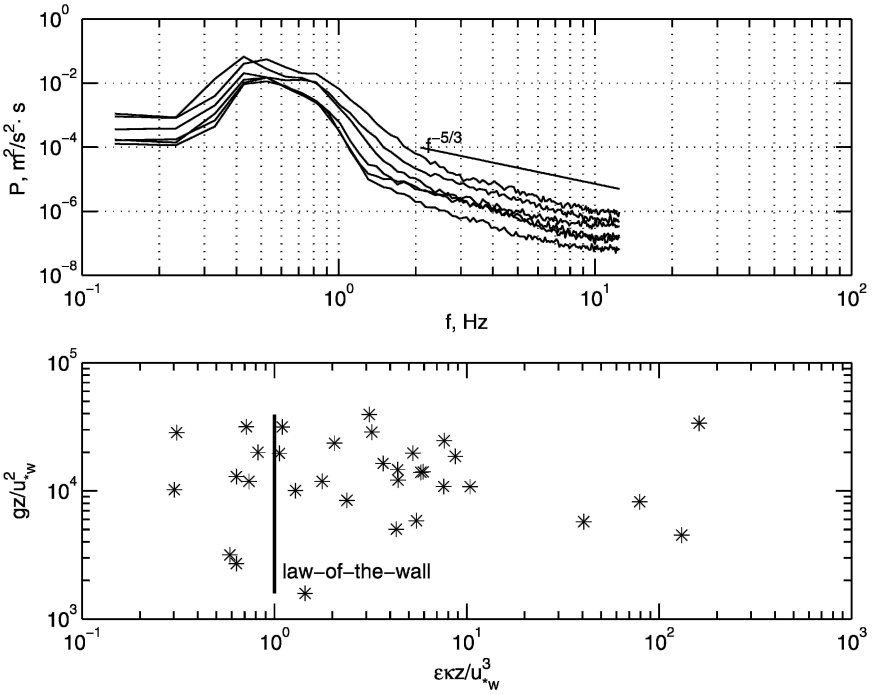

FIG. 11. ADV measurements of dissipation rates: (top) six spectra measured at distances from 10 cm from the surface (top spectrum) to 60 cm from the surface (bottom spectrum); (bottom) "law-of-the-wall" coordinates.

direct measurement of the wave-induced bottom shear stress. These measurements were to be made with a special-purpose bottom-mounted shear plate. A laboratory version of the plate had been developed and successfully tested. A flat plate was mounted on spring elements that allowed the plate to translate horizontally under the applied shear stress. The displacement of the plate (less than 0.5 mm) was linearly related to the imposed shear stress and was sensed with a high-resolution proximity gauge.

However, the nature of the Lake George bed sediments prevented the field version of the shear plate from operating successfully. The Lake George bed material consists of a thick layer of fine cohesive silt, which quickly impeded movement of the mobile parts of the plate. As a result, a combination of laboratory tests and field measurements was used to estimate the bottom-dissipation function, S_{bf} in Eq. (1).

Comprehensive measurement of the spectral distribution of S_{bf} as a function of the wave spectrum, water depth, and bottom roughness were performed in the large wave tank of the School of Civil Engineering, ADFA (Mirfenderesk and Young 2004). The shear plate, a laser Doppler velocimeter, and an ADV with a reduced 1-mm sampling volume were used. The ADV was transferred to the Lake George site during AUSWEX, and accurate measurements of velocity profiles in the bottom boundary layer were taken with a high-precision vertical traversing system in an attempt to obtain bottom-roughness properties for the Lake George bed. Values of the bottom roughness, combined with the Mirfenderesk and Young (2004) dependence of S_{bf} on wave and depth conditions, then allowed an estimate of the bottom-friction function.

Direct measurements of the bottom-friction factor were also obtained. Approximately 2 tons of the bed material were transferred to a laboratory flume to cover its entire floor with a 20-cm layer. A range of boundary layer measurements was conducted for unidirectional flow velocities. One such boundary layer profile, for a mean flow above the boundary layer $u_{max} = 0.13\ m\ s^{-1}$, is shown in Fig. 12a. The bottom boundary layer is clear, with both turbulent and viscous sublayers. Logarithmic profiles were fit to such boundary layer profiles to determine the bed roughness.

The range of u_{max} used in the laboratory tests covered a broad span of flow conditions in the bottom boundary layer, for which Nikuradze roughness parameter k_s was inferred. Nikuradze roughness k_s, even though it has dimension of length, does not describe directly size, shapes, or spatial distributions of the protrusions of a particular bottom bed. It is a dimension of uniform sand grains that would have the same effect on the water flow as the present bottom formation. It is a

Unauthenticated | Downloaded 10/04/22 07:42 PM UTC

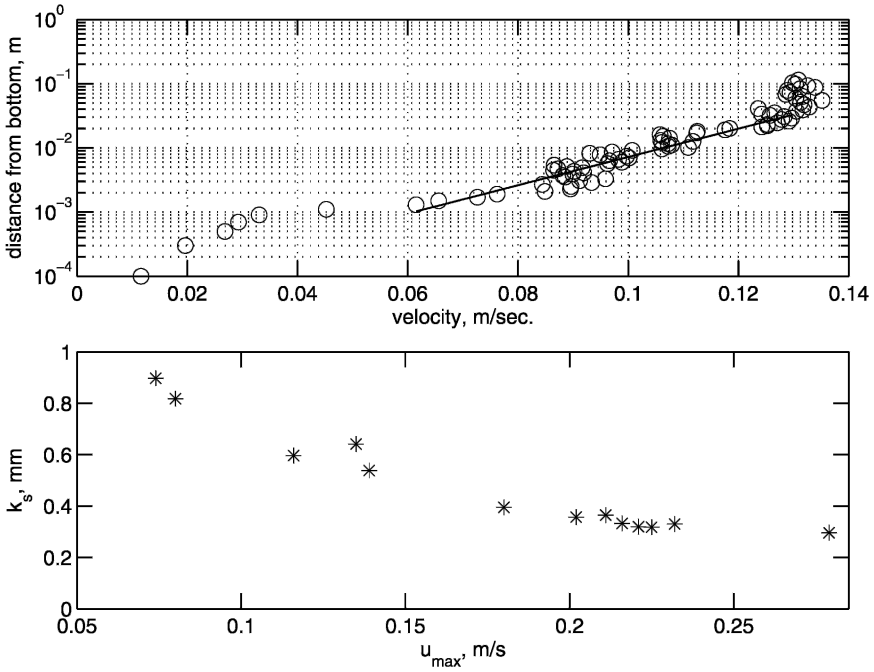

FIG. 12. Roughness measurements for the Lake George bottom silt. (a) Mean velocity profile for $u_{\max} = 0.13$ m s^{-1}. (b) Nikuradze roughness k_s vs $u_{\max}$ below ripple formation state.

convenient measure that can be obtained from the boundary layer velocity profiles and then used to estimate the bottom friction and ultimately the dissipation due to bottom friction. Figure 12b shows the Nikuradze roughness parameter k_s as a function of $u_{\max}$ up to $u_{\max} = 0.285$ cm s^{-1}.

At $u_{\max} \approx 0.285$ m s^{-1}, ripples formed on the bed and k_s increased by more than an order of magnitude (this sudden jump is not shown for the clarity of the figure). At the measurement site, there was no evidence of ripple formation. However, immediately shoreward of the field measurement site, ripples were evident. Hence, it can be concluded that the bed roughness at the measurement site was close to the transition to ripple formation. As k_s does not vary significantly with increasing $u_{\max}$ in this region, it has been assumed that $k_s \approx 0.3$ mm for the field site.

e. Determination of nonlinear interactions

Nonlinear interactions involving three, four, and five wave components are all possible in the finite-depth conditions experienced during the experiment. It was not proposed to measure these nonlinear interaction terms directly. Indeed, it appears that direct measurements that could isolate such terms from the other processes are probably not possible. Bispectral analysis can be used to determine the phase coherence within the spectrum that may result from three-wave, or triad, interactions. Such an analysis requires extremely long, yet stationary, time series to obtain statistical confidence. The consistent and homogeneous wind fields, together with the lack of tidal variation, made such measurements possible in the lake. Indeed, Young and Eldeberky (1998) had conducted such an analysis on Lake George data, showing that triad interactions may be significant under these conditions.

All these nonlinear processes can, to some extent, be modeled. In this regard the simple, approximately constant depth fetch-limited conditions will enable one-spatial-dimension models to be utilized. Hence, sophisticated treatment of the nonlinear terms should be possible and yet remain computationally tractable.

The treatment of four-wave nonlinear interaction in deep-water wave models is traditionally formulated in terms of the perturbation theory of Hasselmann (1962). Future analysis of nonlinear effects will concentrate on four-wave interactions, which will be most important in the "intermediate depth" conditions of Lake George. The nonlinear code of Tracy and Resio (1982) and its advanced modification (WAVETIME-1; G. van Vledder, Alkyon, 2002, personal communication) will be used for this purpose.

f. Integration of all systems

Field instrumentation is always difficult. The research platform, however, provided a convenient work-

Unauthenticated | Downloaded 10/04/22 07:42 PM UTC

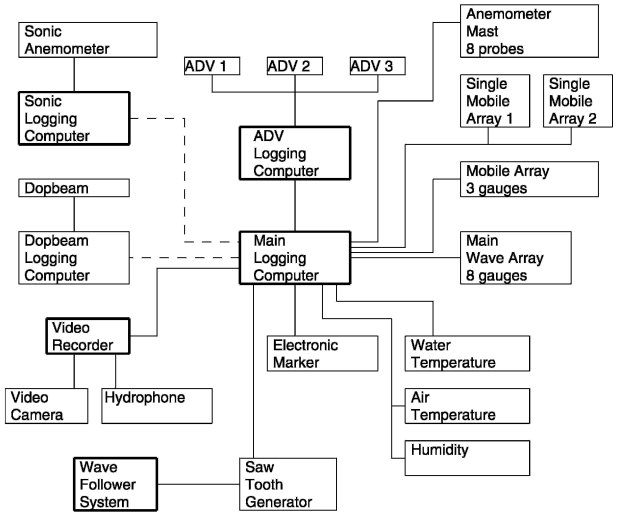

FIG. 13. Diagram of the integrated set of Lake George instrumentation. Thicker lines indicate master devices, which control and read other instruments. Dotted lines indicate systems, which are synchronized with the main logging computer by clock only.

ing environment for the deployment of all instrumentation. The experiment required the measurement of a large number of quantities, as shown in Fig. 13 (list of all acronyms used is provided in the appendix). In addition, a key element of the project was to simultaneously measure as many of the source terms as possible. As a result, the data acquisition system was designed to simultaneously log all the various measurements.

As seen in Fig. 13, the main logging computer controlled synchronization of all the measurements. It either logged the measured quantities itself or sent synchronization pulses to other devices, which controlled and logged particular measurements and readings (shown with thicker lines in the diagram). A single PC with a 64-channel A/D board was used as the main computer to log all the analog outputs together with the time codes of the video recorder 25 times per second.

The ADVs and the sonic anemometer both had their separate controlling and logging computers. Both the ADVs and the sonic anemometer were deployed to measure turbulent quantities and came with dedicated PC boards that enabled digital transfer of data. Experience with these instruments showed that this form of data acquisition was preferable to the use of analog outputs. Indeed the available signal-to-noise ratio made the recovery of high-frequency components of the spectrum impossible with analog data acquisition for these instruments. All other quantities were measured adequately with analog outputs.

The ADV controlling computer was sent a synchronization pulse by the main computer 25 times per second, and therefore its recordings had absolute synchronization with most of the data. The sonic anemometer board had a 21-Hz digitizing rate and could not have been synchronized with the main computer directly. Therefore, to provide time cross-reference, the clocks of the two computers were synchronized and starting times of all the records were registered. Independent operation of the sonic anemometer also made sense, since continuous records of much longer duration, compared to the other measurements, were usually required to obtain reliable estimates of stress variations in the boundary layer.

During AUSWEX, Dopbeam measurements were set up [see section 3c(3)]. The Dopbeam had high memory capacity requirements and internal limitations, which did not allow records in excess of 4-min length, and recorded turbulence profiles at a rate of 25 Hz. Therefore, its logging was organized on a separate computer, synchronized by clock with the rest of measurements, as was done for the sonic anemometer.

The video recording has been mentioned many times above. The mobile video camera, with cable connected to a Panasonic Professional SVHS Video Recorder AG-7350, was used for recording waves in the vicinity of the main wave array, detecting breaking events, observing evolution of wave groups, taping the wave follower in action, etc. The AG-7350 provided video sampling at a 25-Hz rate, the same as most of the other measurements, and absolute synchronization with the other measurements by means of time coding of each video frame, which was both recorded on the video tape and transmitted to the main computer and logged in the main data file along with other readings. To start and stop the video recording, a synchronization pulse from the main computer was used, as seen in the diagram. The video recorder had two audio channels, one of which was used for the time code recording and the other one for synchronous recording of analog output of the subsurface hydrophone.

The multipurpose and multichannel wave-follower system, set up during AUSWEX, had its own registration system, as described in Donelan et al. (2005). Its sampling frequency was 50 Hz, and it was synchronized with the main logging computer of the rest of Lake George measurements by means of a sawtooth generator, whose signal was recorded both by the wave follower and by the main logging computer.

The quantities measured and probes used are detailed below.

Unauthenticated | Downloaded 10/04/22 07:42 PM UTC

- *Directional wave subsystem*
  Eight capacitance probes (main array)
  Three resistance probes (mobile array)
  Two mobile arrays of a single capacitance probe
- *Atmospheric input subsystem*
  Boundary layer array—six anemometer wind speed channels (plus four wind gust channels), two wind direction channels
  Sonic anemometer—digital output to dedicated PC
  Wave follower—pressure at water surface measured by Elliott probe, position of wave follower, water surface elevation (one resistance wire and three capacitance probes), two Pitot tubes, two hot films, three bottom pressure probes, wind vane, dedicated hydrophone, synchronization with the main logging computer (see Donelan et al. 2005)
  Air temperature
  Water temperature
  Air humidity
- *WhiteCap dissipation subsystem*
  Acoustic Doppler velocimeters—three digital outputs to dedicated PC, digital synchronization line to main A/D system
  Video—time codes recorded via RS232 line
  Water surface elevation—13 wave gauge outputs
  Hydrophone—one analog output
  Wave-follower hydrophone—one digital output
  Electronic marker
- *Bottom friction subsystem*
  Acoustic Doppler velocimeter with reduced sample volume—one digital output to dedicated PC, digital synchronization to main A/D system
- *Synchronizations*
  Digital synchronization with ADV recording computer
  Time code synchronization with video system
  Sawtooth generator signal as synchronization with wave-follower system
  Clock synchronization with sonic anemometer recording computer
  Clock synchronization with Dopbeam recording computer
- *Other*
  Mean current measurements by subsurface ADVs

g. Data formats

Data from the Lake George site were obtained for 3 yr, including the intensive AUSWEX period. A database, containing hundreds of hours of wave, wind, air turbulence, subsurface currents and turbulence, underwater sound, humidity, air and water temperatures, and other records, as well as photographic images of the surface, was prepared, documented, and is available on seven CDs. About 90 h of relevant video and hydrophone sound records, with synchronizing time codes, are available on two sets of 30 SuperVHS videotapes.

The joint AUSWEX experiment was carried out from 14 August to 18 September 1999. The data acquired comprise numerous synchronized records by the wave array, anemometer masts, sonic anemometer, three ADVs located at different levels in the water column, video camera, hydrophone, humidity and temperature probes, as well as by the Dopbeam, which was traversed to different depths, and by the wave follower. These data comprise four CDs and about 45 h of video and hydrophone sound records.

Most of the data are available as tabulated ASCII codes. A number of analog hydrophone records, which were digitized at 8-kHz rates, are archived and available on the CDs as binary codes. The Dopbeam records are also stored in binary format.

4. Discussion

A field experiment was described, with the long-term goal of obtaining closure of the energy balance equation for wind-wave evolution in finite-depth water by means of direct measurement of the main source terms. These source terms represent the basic physical processes required to develop reliable finite-depth wave prediction models (Young and Babanin 2001).

a. Unique nature of the experiment

The experiment was at a significantly smaller scale than traditional oceanographic field experiments. This enabled a far more controlled experimental design. The scale of the experiment was, however, such that the conditions measured were representative of coastal ocean situations. As was stated above, wave conditions at the site were intermediate-water-depth wind seas with wave ages from young to moderate. Specific advantages of the experimental location are detailed below.

The relatively small spatial extent of the lake means that experimental conditions could have been chosen with near-homogeneous and well-defined wind fields.

The simple bathymetry and close approximation to ideal fetch-limited conditions make model intercomparison and model-aided interpretation of the data relatively straightforward.

The absence of swell will simplify the interpretation of nonlinear interactions. Indeed, the results from

Unauthenticated | Downloaded 10/04/22 07:42 PM UTC

this experiment will complement open ocean experiments and aid in the interpretation of results from more complex sea conditions.

The absence of tidal variation and the consistent westerly winds that occur in the region during winter facilitated the measurement of extremely long, yet stationary, time series. Such time series can be analyzed using bispectral techniques to determine the importance of triad interactions.

Once the experimental facility was developed, experiments could be repeated as required. This enabled the gradual refinement of experimental techniques and ensured a high data return. This is a luxury not available in traditional ship-based experiments.

The scale of the experiment enabled relatively fragile equipment to be deployed. Examples of such instrumentation are the high-precision and high-frequency wave-follower system and laboratory versions of acoustic Doppler velocimeters. The operation of such instruments in the open ocean would be extremely difficult.

b. Integration with SHOWEX

The described measurement program was complementary to and integrated with the larger open ocean Shoaling Waves Experiment (SHOWEX). Both experiments were designed to study wave generation, development, and propagation in finite-depth environments, although at different scales.

The SHOWEX data were obtained in the open ocean and dealt with real-size ocean waves in their typical environment. Measurements of fine effects driving wave generation and dissipation, however, are difficult and often impossible during such conditions. For example, it is not possible to use a precise wave-following technology from research vessels and therefore to conduct detailed air–sea interaction measurements at small scales, where these interactions are most significant.

Lake George data correspond to more simple fetch-limited conditions, single-point measurements and physically much smaller and shorter waves. These are, however, field data, for the waves generated and developed in their natural environment, which allow the investigation in greater detail of phenomena studied at a larger scale in the open ocean during SHOWEX.

5. Conclusions: Analyses completed and future plans

The Lake George field experiment was a long-term program, having started in September 1997 and formally finished in August 2000, when the measurements ceased and the site was dismantled. However, while the field measurements were still in progress, data analyses had begun and have continued since. A number of results on bimodality of wave spectra, wind input, surface drag and roughness, breaking statistics, dissipation function, bottom interaction and bottom friction, nonlinear effects in the air–sea interaction, and total energy balance in the wave field have already been presented and published, as indicated in the references throughout the present paper.

In the near future, based on the Lake George experiment, we plan to develop parameterizations of the spectral functions of the wind input S_{in}; whitecapping dissipation S_{ds}; bottom friction S_{bf} Eq. (1) in terms of the wave field and environmental properties, including shallow water versions for the first two terms; and verification of the total spectral energy balance taking account of nonlinear interactions. The source terms will then be incorporated into a wave model.

More specific studies, utilizing the Lake George data, are being conducted on issues of wind-input enhancement due to wave breaking, directional wavenumber spectra, directionality and severity of breaking events, and alteration of near-surface dissipation due to wave breaking.

Acknowledgments. The authors gratefully acknowledge the financial support of the U.S. Office of Naval Research (Grants N00014-97-1-0234, N00014-97-1-0277, and N00014-97-1-0233) and the Australian Research Council (Grant A00102965). We also express our gratitude to the staff and students of the School of Civil Engineering of the Australian Defence Force Academy—Jim Baxter, Michael Jones, Mary Dalton, Michael Lanza, John MacLeod, Hamid Mirfenderesk, Bernard Miller, Karl Shaw, Ian Shepherd, and Michael Wilson—who offered highly professional and prompt responses to all urgent demands during the experiment. We are also very grateful to CSIRO, Canberra, and the School of Aerospace and Mechanical Engineering, ADFA, for their assistance with calibrations of the wind probes.

APPENDIX

Acronyms Used

ADFA	Australian Defence Force Academy
ADV	Sontek acoustic Doppler velocimeter [section 3c(2)]

Unauthenticated | Downloaded 10/04/22 07:42 PM UTC

AUSWEX	Australian Shallow Water Experiment
Dopbeam	Pulse-to-pulse coherent acoustic Doppler profiler (Veron and Melville 1999)
DSTO	Australian Defence Science and Technology Organization
Elliott probe	Elliott pressure disk (Elliott 1972)
HTI-96-MIN hydrophone	High Tech, Inc., hydrophone model [section 3c(1)]
MLM	Maximum likelihood method to compute wave directional spectra (Capon 1969)
Sonic anemometer	Gill Instruments Solent Research ultrasonic anemometer (section 3b)
TMA spectrum	Finite-depth wave spectrum based on TMA dataset (Bouws et al. 1985)
WDM	Wavelet directional method to compute wave directional spectra (Donelan et al. 1996)
WG-30	Richard Brancker wave gauge system (section 3a)

REFERENCES

Agrawal, Y. C., E. A. Terray, M. A. Donelan, P. A. Hwang, A. J. Williams III, W. M. Drennan, K. K. Kahma, and S. A. Kitaigorodskii, 1992: Enhanced dissipation of kinetic energy beneath surface waves. *Nature,* **359,** 219–220.

Babanin, A. V., and Y. P. Soloviev, 1998: Variability of directional spectra of wind-generated waves, studied by means of wave staff arrays. *Mar. Freshwater Res.,* **49,** 89–101.

——, I. R. Young, and M. L. Banner, 1999: An observational investigation of bimodal directional spreading of fetch-limited waves. *The Wind-Driven Air–Sea Interface,* M. L. Banner, Ed., The University of New South Wales, 7–8.

——, ——, and ——, 2001: Breaking probabilities for dominant surface waves on water of finite constant depth. *J. Geophys. Res.,* **106,** 11 659–11 676.

Bouws, E., H. Gunther, W. Rosenthal, and C. L. Vincent, 1985: Similarity of the wind wave spectrum in finite depth water, Part I. Spectral form. *J. Geophys. Res.,* **90,** 975–986.

Bretschneider, C. L., 1958: Revised wave forecasting relationships. *Proc. Sixth Conf. on Coastal Engineering,* Los Angeles, CA, ASCE, 30–67.

Capon, J., 1969: High-resolution frequency–wavenumber spectrum analysis. *Proc. IEEE,* **57,** 1408–1418.

Craig, P. J., and M. L. Banner, 1994: Modeling wave-enhanced turbulence in the ocean surface layer. *J. Phys. Oceanogr.,* **24,** 2546–2559.

Donelan, M. A., 1990: Air–sea interaction. *The Sea,* B. LeMehaute and D. M. Hanes, Eds., Ocean Engineering Science, Vol. 9, Wiley and Sons, 239–292.

——, 1999: Wind-induced growth and attenuation of laboratory waves. *Wind-over-Wave Couplings,* S. G. Sajjadi, N. H. Thomas, and J. C. R. Hunt, Eds., 183–194.

——, J. Hamilton, and W. H. Hui, 1985: Directional spectra of wind-generated waves. *Philos. Trans. Roy. Soc. London,* **A315,** 509–562.

——, W. M. Drennan, and A. K. Magnusson, 1996: Nonstationary analysis of the directional properties of propagating waves. *J. Phys. Oceanogr.,* **26,** 1901–1913.

——, N. Madsen, K. K. Kahma, I. K. Tsanis, and W. M. Drennan, 1999: Apparatus for atmospheric surface layer measurements over waves. *J. Atmos. Oceanic Technol.,* **16,** 1172–1182.

——, A. V. Babanin, I. R. Young, M. L. Banner, and C. McCormick, 2005: Wave-follower field measurements of the wind-input spectral function. Part I: Measurements and calibrations. *J. Atmos. Oceanic Technol.,* **22,** 799–813.

Drennan, W. M., M. A. Donelan, K. B. Katsaros, and E. A. Terray, 1996: Oceanic turbulence dissipation measurements in SWADE. *J. Phys. Oceanogr.,* **26,** 808–815.

Elliott, J. A., 1972: Instrumentation for measuring static pressure fluctuations within the atmospheric boundary layer. *Bound.-Layer Meteor.,* **2,** 476–495.

Hasselmann, K., 1962: On the nonlinear energy transfer in a gravity-wave spectrum, Part I. General theory. *J. Fluid Mech.,* **12,** 481–500.

Loewen, M. R., and W. K. Melville, 1991 Microwave backscatter and acoustic radiation from breaking waves. *J. Fluid Mech.,* **224,** 601–623.

Lumley, J. L., and E. A. Terray, 1983: Frequency spectra of frozen turbulence in a random wave field. *J. Phys. Oceanogr.,* **13,** 2000–2007.

Melville, W. K., 1994: Energy dissipation by breaking waves. *J. Phys. Oceanogr.,* **24,** 2041–2049.

——, M. R. Loewen, F. C. Felizardo, A. T. Jessup, and M. J. Buckingham, 1988: Acoustic and microwave signatures of breaking waves. *Nature,* **336,** 54–59.

Mirfenderesk, H., and I. R. Young, 2004: Direct measurements of the bottom friction factor beneath surface gravity waves. *Appl. Ocean Res.,* **25,** 269–287.

Rapp, R. J., and W. K. Melville, 1990: Laboratory measurements of deep-water breaking waves. *Philos. Trans. Roy. Soc. London,* **A331,** 735–800.

Snyder, R. L., F. W. Dobson, J. A. Elliott, and R. B. Long, 1981: Array measurements of atmospheric pressure fluctuations above surface gravity waves. *J. Fluid Mech.,* **102,** 1–59.

Soloviev, A. V., N. V. Vershinskiy, and V. A. Bezverchnii, 1988: Small-scale turbulence measurements in the thin surface layer of the ocean. *Deep-Sea Res.,* **35,** 1859–1874.

Terray, E. A., M. A. Donelan, Y. Agrawal, W. M. Drennan, K. K. Kahma, A. J. Williams, III, P. A. Hwang, and S. A. Kitaigorodskii, 1996: Estimates of kinetic energy dissipation under breaking waves. *J. Phys. Oceanogr.,* **26,** 792–807.

Tracy, B., and D. T. Resio, 1982: Theory and calculation of the nonlinear energy transfer between sea waves in deep water. U.S. Army Engineer Waterways Experiment Station Rep. 11, Vicksburg, MS, 50 pp.

Veron, F., and W. K. Melville, 1999: Pulse-to-pulse coherent Doppler measurements of waves and turbulence. *J. Atmos. Oceanic Technol.,* **16,** 1580–1597.

Weber, S. L., 1991: Bottom friction for wind sea and swell in extreme depth-limited situations. *J. Phys. Oceangr.,* **21,** 149–172.

Young, I. R., 1994: On the measurement of directional wave spectra. *Appl. Ocean Res.,* **16,** 283–294.

Unauthenticated | Downloaded 10/04/22 07:42 PM UTC

——, 1999: *Wind Generated Ocean Waves.* Elsevier, 288 pp.

——, and R. J. Sobey, 1985: Measurements of the wind-wave energy flux in an opposing wind. *J. Fluid Mech.,* **151,** 427–442.

——, and L. A. Verhagen, 1996a: The growth of fetch limited waves in water of finite depth. Part I: Total energy and peak frequency. *Coastal Eng.,* **29,** 47–78.

——, and ——, 1996b: The growth of fetch limited waves in water of finite depth. Part II: Spectral evolution. *Coastal Eng.,* **29,** 79–100.

——, and Y. Eldeberky, 1998: Observations of triad coupling of finite depth wind-waves. *Coastal Eng.,* **33,** 137–154.

——, and A. V. Babanin, 2001: Wind wave evolution in finite depth water. *Proc. 14th Australasian Fluid Mechanics Conf.,* Adelaide, Australia, Australian Mathematical Society, 79–86.

——, L. A. Verhagen, and S. K. Khatri, 1996: The growth of fetch limited waves in water of finite depth. Part III: Directional spectra. *Coastal Eng.,* **29,** 101–121.

——, M. A. Dalton, P. J. McMahon, and L. A. Verhagen, 1997: Design of integrated shallow water wave experiment. *IEEE J. Oceanic Eng.,* **22,** 184–188.

Unauthenticated | Downloaded 10/04/22 07:42 PM UTC